Proceedings of Computational Engineering Conference JSCES
Vol. 29, 2024 May

Optimizing the airflow of displacement ventilation system to reduce the risk of particle inhalation and energy usage.

Rahul Bale [1) 2)] Haruki Nakagawa [3)] Alicia Muruga [4)] and Tsubokura Makoto [5) 6)]

[1)]Graduate School of System Informatics, Kobe University (Kobe, Japan.)
[2)]RIKEN Center for Computational Science (Kobe, Japan, E-mail: rahul.bale@riken.jp)
[3)]Graduate School of System Informatics, Kobe University (Kobe, Japan.)
[4)]Graduate School of System Informatics, Kobe University (Kobe, Japan.)
[5)]RIKEN Center for Computational Science (Kobe, Japan.)
[6)]Graduate School of System Informatics, Kobe University (Kobe, Japan. , E-mail: mtsubo@riken.jp)

In this study, we explored optimizing indoor ventilation systems to mitigate aerosol transmission risks highlighted by the COVID-19 pandemic. We assessed the potential of retrofitting existing mixed ventilation systems with displacement ventilation, which introduces fresh air from below to efficiently remove airborne contaminants. Utilizing droplet simulations with the CUBE solver and genetic algorithms for design optimization, we balanced infection risk reduction against energy consumption. Our results demonstrated significant droplet concentration reductions in optimized scenarios, highlighting a trade-off between health risks and energy use, as evidenced by the generated Pareto curve.

Key Words : *COVID, Indoor Ventilation, Optimization*

1. INTRODUCTION

The novel coronavirus, identified in 2019, spread globally, significantly impacting public health systems and everyday life. One of the factors contributing to the rapid expansion of COVID-19 infections is the lengthy asymptomatic incubation period during which unaware carriers can transmit the virus to others. This characteristic made it challenging to identify and isolate infected individuals promptly, complicating efforts to control the spread of the disease. The virus primarily transmits through three pathways: contact, droplet, and aerosol transmission. Contact transmission occurs when virus-laden droplets from an infected individual contaminate another person's hands, which then contact mucous membranes. Droplet transmission involves direct mucosal deposition from larger respiratory droplets, while aerosol transmission occurs through inhalation of microscopic droplets suspended in the air.

Addressing these modes of transmission has involved various strategies: hand hygiene using alcohol-based sanitizers for contact transmission, wearing masks and avoiding crowded places for droplet precautions, and enhancing ventilation for aerosol transmission. However, maintaining social distancing is not always feasible in everyday life, making effective ventilation an essential strategy, particularly against aerosol transmission.

Most facilities typically employ mixed ventilation systems that dilute and disperse indoor pollutants by mixing contaminated indoor air with fresh intake. However, this method is less effective in clearing smaller aerosol particles that pose a significant infection risk. An alternative, displacement ventilation, introduces fresh air at a lower level, allowing natural convection to lift lighter airborne contaminants to upper exhaust outlets without mixing with the indoor air. This method can effectively ventilate pollutants but has been limited by high costs. In his research, Yamamoto addressed these cost challenges by adapting traditional mixed ventilation systems for displacement ventilation, achieving successful replication but not yet examining more efficient designs comprehensively. This background sets the stage for our study, which aims to further explore and optimize ventilation designs to enhance public health safety efficiently.

2. GOVERNING EQUATIONS

The sputum droplet dispersion is modelled through a combination of a Lagrangian frame for the droplet dynamics and the air/gas flow dynamics are modelled on a conventional fixed Eulerian mesh. The conservation equations for mass, momentum, energy are solved on the Eulerian mesh. Species transport equations are considered to account for the humidity variation around the mouth during a cough. The conservation equations in the compact form are given by

$$\frac{\partial \mathrm{U}}{\partial t} + \nabla \cdot \mathbf{F} = \mathbf{S}, \tag{1}$$

where U and $\mathbf{F}$ are given below.

© 一般社団法人日本計算工学会

$$\mathrm{U} = \begin{pmatrix} [1.25]\rho \\ \rho u_1 \\ \rho u_2 \\ \rho u_3 \\ \rho e \\ \rho Y_k \end{pmatrix}, F_i = \begin{pmatrix} [1.25]\rho u_i \\ \rho u_i u_1 + P\delta_{i1} - \mu A_{i1} \\ \rho u_i u_2 + P\delta_{i2} - \mu A_{i2} \\ \rho u_i u_3 + P\delta_{i3} - \mu A_{i3} \\ \rho(\rho e + P)u_i - \mu A_{ij}u_j + q_i \\ \rho u_i Y_k - \rho \hat{u}_i^k Y_k \end{pmatrix},$$

$$\mathbf{S} = \begin{pmatrix} 0 \\ (\rho - \rho_0)g_1 \\ (\rho - \rho_0)g_2 \\ (\rho - \rho_0)g_3 \\ (\rho - \rho_0)g_i u_i \\ S_{\rho Y_k} \end{pmatrix}. \tag{2}$$

Here, the density of the gas/air is represented by ρ and the viscosity is given by μ. $\mathbf{u}$, e and P represent the velocity, total specific energy and the pressure, respectively. Species mass fraction and diffusion velocities of the k^{th} species are given by Y_k and $\hat{u}_i^k$, respectively. (u_1, u_2, u_3) are the components of the velocity vector $\mathbf{u}$ along the principal directions $1, 2, 3$. $\mathbf{g}$ is the acceleration due to gravity (eg. $\mathbf{g} = (0, 0, -9.81)m/s^2$). Of the species source terms $S_{\rho Y_k}$, the non-droplet vapor species are zero. The definition of the total specific energy is given by the following equation

$$e = \frac{P}{\gamma - 1} + \frac{1}{2}u_i u_i, \tag{3}$$

where γ is the ratio of the gas specific heat capacities. The heat flux $\mathbf{q}$ is given by

$$\mathbf{q} = -\lambda \nabla T, \tag{4}$$

where λ is the thermal diffusivity, and $\mathbf{A}$ is the velocity gradient tensor. The diffusion velocities of the chemical species may be expressed as a function of species diffusivity D_k as

$$\hat{\mathbf{u}}^k Y_k = D_k \nabla Y_k. \tag{5}$$

(1) Droplet Model

We adopt a one-way coupling approach for the droplet transport and evaporation model, wherein it is assumed that the effect of droplet motion and evaporation on the ambient air is negligible while the droplet transport and evaporation are directly linked to the airflow and temperature [3]. The equations modelling the transport, evaporation and the rate of change of droplet temperature are given by the equations below

Given below are the equations governing the rate of change of droplet mass, m_d, velocity, $\mathbf{u}_d$, temperature, T_d and position.

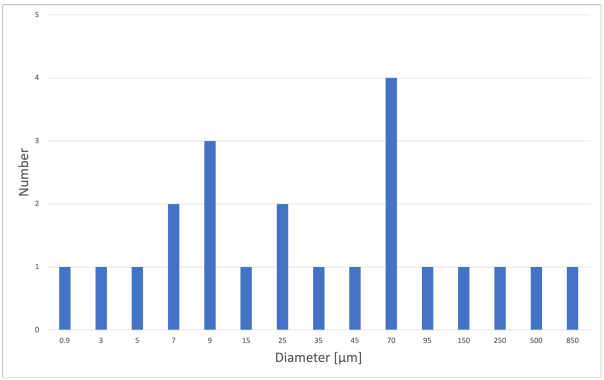

Fig. 1 a) Distribution of droplet diameter at the time of injection[1].

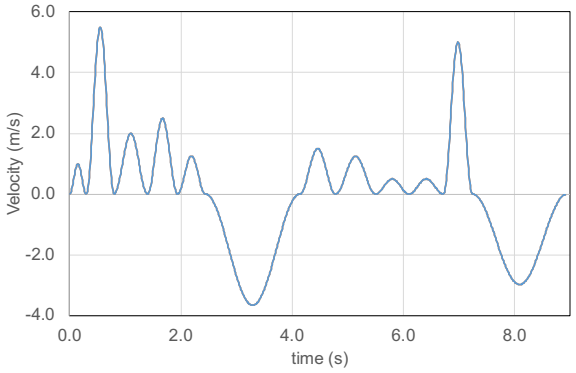

Fig. 2 The velocity profile of flow generated during the speech as function of time[2].

$$\frac{d\mathbf{x}_d}{dt} = \mathbf{u}_d, \tag{6}$$

$$\frac{d\mathbf{u}_d}{dt} = \frac{3C_D}{4d_d}\frac{\rho}{\rho_d}(\mathbf{u} - \mathbf{u}_d)|\mathbf{u} - \mathbf{u}_d|, \tag{7}$$

$$\frac{dT_d}{dt} = \frac{Nu}{3Pr}\frac{c_p}{c_l}\frac{f_1}{\tau_d}(T - T_d) + \frac{1}{m_d}\left(\frac{dm_d}{dt}\right)\frac{L_V}{c_{p,d}}, \tag{8}$$

$$\frac{dm_d}{dt} = -\frac{m_d}{\tau_d}\left(\frac{Sh}{3Sc}\right)\ln(1 + B_M). \tag{9}$$

Here, $\mathbf{x}_d$, $\mathbf{u}_d$, m_d, and T_d are the droplet position, velocity, mass and temperature, respectively. T is the temperature of the ambient air, L_v the latent heat of evaporation at the droplet temperature. c_p and c_l are the specific heat at constant pressure of the ambient air and the specific heat capacity of the liquid droplet, and τ_d is the response time of the droplet. f_1 is a correction to the heat transfer due to evaporation of the droplet[4]. Nu & Pr are the Nusselt and Prandtl numbers, respectively [5,6]. B_m is the mass transfer number (details of which can be found in [3]), and Sh & Sc are the Sherwood and Schmidt numbers, respectively. Under a unit Lewis number assumption $Pr = Sc$. For the evaluation of the Prandtl number the standard definition is used, where as

© 一般社団法人日本計算工学会

the Nusselt number [7,8] is evaluated using the expression is given below along with the definition of τ_d.

$$\tau_d = \frac{\rho_d d_d^2}{18\mu} \tag{10}$$

$$Nu = 2 + 0.552 Re_s^{1/2} Pr^{1/3} \tag{11}$$

$$Sh = 2 + 0.552 Re_s^{1/2} Sc^{1/3} \tag{12}$$

In the above equation ρ_d is the density of the droplet and Re_s is the Reynolds number based on the slip velocity of a droplet with respect to the gas phase flow velocity, $\mathrm{u_{slip}} = \max(|\mathbf{u} - \mathbf{u_d}|)$

$$Re_s = \frac{\rho \mathrm{u_{slip}} \mathrm{d_d}}{\mu}. \tag{13}$$

The drag coefficient of the droplet, C_D, depends on its Reynolds number and is given by

$$C_D = \begin{cases} \frac{24}{Re_d}\left(1 + 1/6 Re_d^{2/3}\right) & Re_d < 1000, \\ 0.424 & Re_d > 1000, \end{cases} \tag{14}$$

and the droplet Reynolds number is given by

$$Re_d = \frac{\rho(\mathbf{u} - \mathbf{u}_d) d_d}{\mu}. \tag{15}$$

3. Simulation Setup

In our study, we analyzed a room equipped with a single air supply and exhaust vent, both located on the wall. The layout of the room is designed to simulate the presence of an infected individual to assess the dispersion and concentration of droplets over time. Figure 3 illustrates the configuration of the room.

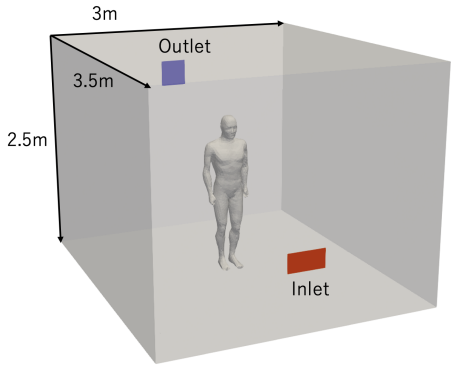

Fig. 3 Ventilation design in the analyzed room.

Air Supply Vent: The design variables for the air supply vent were its size and position. We identified ten potential positions, distributed evenly across the upper and lower sections of the wall. Figure 4 shows these possible positions, facilitating the selection of the optimal placement for effective air distribution. The vent size varied between two options: 0.2×0.4 m^2 and 0.3×0.5 m^2, as summarized in Table 1.

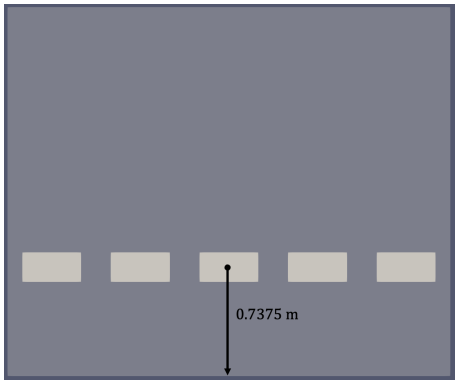

Fig. 4-a Upper inlet

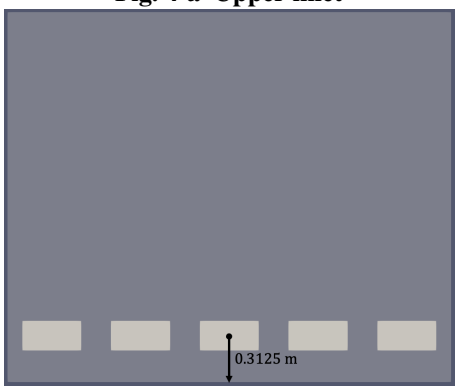

Fig. 4-b Lower inlet

Fig. 4 Potential positions for the air supply vent.

Table 1 Options for air supply vent size.

Case	Size 1 (m^2)	Size 2 (m^2)
1	0.2×0.4	0.3×0.5

Exhaust Vent: The exhaust vent's size and position were determined using a similar methodology as the supply vent. Figure 5 and Table 2 outline these variables to ensure a balanced ventilation approach.

Table 2 Exhaust vent size options.

Case	Size 1 (m^2)	Size 2 (m^2)
1	0.2×0.4	0.3×0.5

This configuration allows us to extensively test the impacts of vent position and size on the efficiency of the ventilation system, aiming to optimize particle dispersion and energy usage.

Flow Rate: For the assessment of our displacement ventilation system, we established a range of flow rates at the inlet vent, incrementally set from 0.01 m³/s to 0.06 m³/s in steps of

© 一般社団法人日本計算工学会

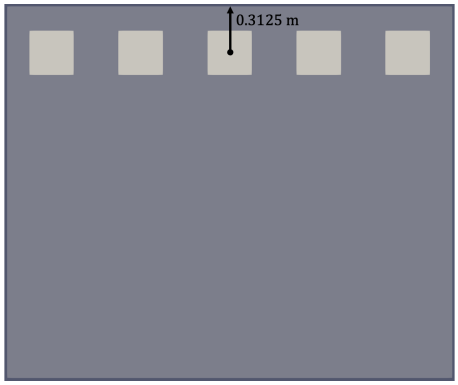

Fig. 5-a Upper outlet

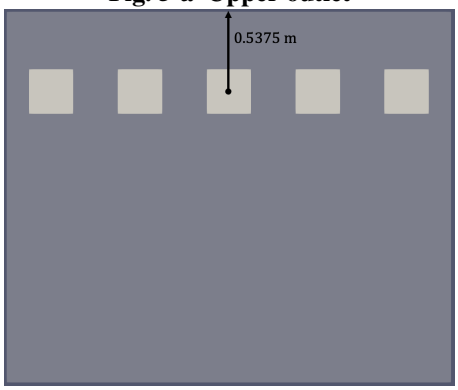

Fig. 5-b Lower outlet

Fig. 5 Configurations for the exhaust vent placement.

0.01 m³/s. This methodical approach allowed us to systematically evaluate the performance of the ventilation system across a spectrum of potential airflow scenarios, ensuring a comprehensive analysis of its effectiveness in various operational conditions. Each incremental step provided a discrete data point for analysis, contributing to a robust set of simulations that informed our optimization strategy.

4. Results

The Pareto optimization analysis conducted on the displacement ventilation system demonstrated a progressive refinement of solutions across six generations. The resulting data, as illustrated in Figure 6, reveals a clear Pareto frontier emerging by the 6th generation, signifying an efficient trade-off between the two competing objectives: virus density and power consumption.

The objective functions of power and virus density (copies/m³) were plotted, where each generation is represented by a distinct color. Initially, in the 1st generation, a wide dispersion of solutions was observed, with some designs yielding low virus density at high power consumption and others showing the opposite trend. Subsequent generations showed a convergence towards a narrow band where the increase in power did not necessarily result in a significant decrease in virus density.

By the 6th generation, represented in red, the data points clustered tightly along a curve, demonstrating that the optimization process had successfully identified designs that strike an optimal balance between minimizing virus density and power usage. Specifically, the solutions with the lowest virus density without excessive power consumption were considered the most favorable.

The stability of the Pareto frontier between the 5th and 6th generations indicates that further iterations did not yield significantly better trade-offs, suggesting a possible convergence of the optimization process. The optimal solutions identified offer insights into the design parameters that contribute to an effective and energy-efficient displacement ventilation system while minimizing the risk of viral particle transmission.

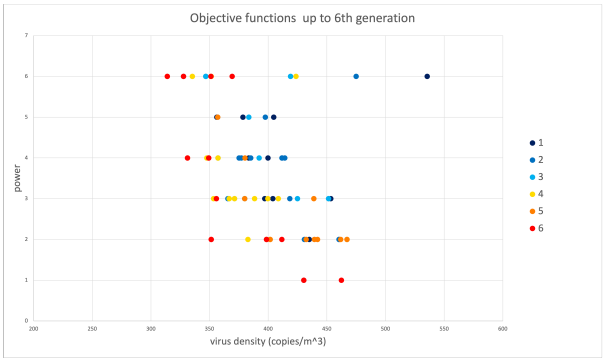

Fig. 6 Pareto Frontier Representing the Trade-off Between Power Consumption (kW) and Virus Density (copies/m³) Across Six Generations.

5. Summary

In this study, we employed Computational Fluid Dynamics (CFD) simulations to evaluate the risk of droplet transmission and utilized the genetic algorithm CHEETAH/R for optimization, aiming to balance infection risk and energy consumption in indoor ventilation systems. As a result, we observed the generation of a Pareto curve through successive generations, demonstrating the feasibility of optimizing ventilation systems using this method. This allows for tailored ventilation designs optimized for specific room configurations, aligning with user-defined priority parameters.

However, this research was limited to a single optimization approach, which precludes a comparative performance analysis with other methods. Future studies should explore different crossover techniques and optimization strategies to evaluate convergence properties and computational costs more comprehensively. Additionally, while this study focused on optimizing infection risk and energy consumption, the aspect of occupant comfort, which is crucial in evaluating ventilation effectiveness, cannot be overlooked. Thus, future

© 一般社団法人日本計算工学会

research should also consider optimizing indoor ventilation with an emphasis on comfort to provide a more holistic approach to ventilation design.

REFERENCES

[1] J. Wei and Y. Li, "Airborne spread of infectious agents in the indoor environment," *American journal of infection control*, vol. 44, no. 9, pp. S102–S108, 2016.
[2] J. K. Gupta, C.-H. Lin, and Q. Chen, "Characterizing exhaled airflow from breathing and talking," *Indoor air*, vol. 20, no. 1, pp. 31–39, 2010.
[3] T. Kitano, J. Nishio, R. Kurose, and S. Komori, "Effects of ambient pressure, gas temperature and combustion reaction on droplet evaporation," *Combustion and Flame*, vol. 161, no. 2, pp. 551–564, 2014.
[4] M. Nakamura, D. Nishioka, J. Hayashi, and F. Akamatsu, "Soot formation, spray characteristics, and structure of jet spray flames under high pressure," *Combustion and Flame*, vol. 158, no. 8, pp. 1615–1623, 2011.
[5] M. Nakamura, F. Akamatsu, R. Kurose, and M. Katsuki, "Combustion mechanism of liquid fuel spray in a gaseous flame," *Physics of Fluids*, vol. 17, no. 12, p. 123301, 2005.
[6] Y. Baba and R. Kurose, "Analysis and flamelet modelling for spray combustion," *Journal of Fluid Mechanics*, vol. 612, pp. 45–79, 2008.
[7] W. Ranz and W. R. Marshall, "Evaporation from drops i," *Chem. eng. prog*, vol. 48, no. 3, pp. 141–146, 1952.
[8] W. Ranz and W. R. Marshall, "Evaporation from drops ii," *Chem. eng. prog*, vol. 48, no. 3, pp. 173–180, 1952.

© 一般社団法人日本計算工学会